Modeling of light transmission under heterogeneous forest canopy: an appraisal of the effect of the precision level of crown description

David Da Silva, Philippe Balandier, Frédéric Boudon, André Marquier, Christophe Godin

Modeling of light transmission under heterogeneous forest canopy: an appraisal of the effect of the precision level of crown description

Number of characters: 51433

Number of tables: 3

Number of figures: 4

Keywords: Light modeling, Forest, Mixed stand, Uneven-aged stand, Canopy description, Multi-scale

David Da Silva & Philippe Balandier & Frédéric Boudon & André Marquier & Christophe Godin

Handling Editor: Erwin Dreyer D. Da Silva (*) Department of Plant Sciences, University of California D

Abstract

- Context: Light availability in forest understorey is essential for many processes, it is therefore a valuable information regarding forest management. However its estimation is often difficult and direct measurements are tedious. Models can be used to compute understorey light but they often require a lot of field data to accurately predict light distribution, particularly in the case of heterogeneous canopies.

- Aims: The influence of the precision level of crown description was studied with a model, MμSLIM, that can be used with both detailed and coarse parametrization with the aim of reducing to a minimum field data requirements.

- Methods: We analyzed the deterioration of the prediction quality of light distribution to the reduction of inputs by comparing simulations to transmitted light measurements in forests of increasing complexity in three different locations.

- Results: With a full set of parameters to describe the tree crown (i.e. crown extension in at least 8 directions, crown height and length), the model accurately simulated the light distribution. Simplifying crown description by a geometric shape with a mean radius of crown extension led to deteriorated but acceptable light distributions. Allometric relationships used to calculate crown extension from trunk DBH seriously reduced light

distribution accuracy.

Introduction

Light in forest understorey is a fundamental resource driving many processes related for example to regeneration growth, vegetation cover and composition, and animal habitat (Balandier *et al.* 2009). Light quality is fundamental for morphogenetic processes, whereas light quantity drives processes linked to carbon acquisition. In this article only light quantity is considered.

For a long time light in forest has only been considered as a factor controlling tree growth, especially in the case of regular even-aged stands in the temperate area. In that context, tree density has been managed to get a very dark understorey with often a bare soil, sign that trees absorbed the maximum of radiations (Perrin 1963). Nowadays a silviculture closer to nature (also named continuous cover forestry) with natural regeneration is promoted or rediscovered (Hale 2009). Irregular uneven-aged stands often with mixed species are managed with partial cutting to create gaps in the forest canopy. These gaps favor some patch of light essential to tree regeneration but also promote the development of understorey vegetation that can compete with young trees and compromise forest dynamic (Balandier *et al.* 2009). Under these conditions, in order to sustain young tree growth while avoiding too dense understorey vegetation, it is essential to proportion light by the size of the gaps (Gaudio *et al.* 2011).

However estimating light quantity in forest understorey is not so easy (Lieffers *et al.* 1999). On one hand, visual assessment are strongly biased by the meteorological conditions, the hour of the day and the operator himself. On the other hand, direct measurements by sensors are often tedious, expensive, require technical competences, and their results also depend on the meteorological conditions and the solar pathway on the day of measurement (Pukkala *et al.* 1993).

Since the pioneer work of Monsi and Saeki (1953), many models simulating light interception and transmission by plant canopies have been developed (see Myneni *et al.,* 1989 and Sillon and Puech, 1994 for reviews) and offer an operative alternative. They are based on, either statistical relationships between vegetation characteristics such as cover, leaf area or leaf area index (LAI) and light transmission, or explicit description of the canopy topology and geometry as elements intercepting light. When forest canopy is homogeneous, i.e. even-aged pure regular stands, statistical models predict mean light quantity in forest understorey with an acceptable accuracy (Balandier *et al.* 2006b; Hale *et al.* 2009; Sonohat *et al.*, 2004). However prediction quality of that type of models decreases drastically with the increase in heterogeneity of the stand structure (Balandier *et al.* 2010). In particular in irregular uneven stands a statistical mean has no sense because it does not reveal the light distribution between understorey and gaps

75 which is of most interest for the forester. With that information, local light
76 availability to favor tree regeneration, plant biodiversity, or animal habitat for
77 example can be estimated (Balandier *et al.* 2006a).
78
79 In that case, complex models with an explicit 3D-description of elements
80 intercepting light give more accurate results. The approach of these models
81 usually involve the use of numerous tracing (sun) rays coming from different
82 points in the sky to a particular point within the stand and compute transmission
83 along those rays taking into account foliage characteristics, thus generating a
84 detailed 2D-map of light availability in the understorey (Cescatti 1997; Brunner
85 1998; Stadt and Lieffers 2000; Courbeau *et al.* 2003; Mariscal *et al.* 2004).
86 However these models require abundant field measurements to parametrize them.
87 These measurements, like a map of tree location on the site, the 3D-geometry of
88 each tree crown with information on leaf area density, distribution and clumping
89 inside the crown, are tedious and often difficult to obtain. Moreover, for
90 management purpose, a detailed 2D-map of light availability in the understorey is
91 not always required. For the forest manager an histogram of light transmittance at
92 the plot level (i.e. percentage of soil per class of transmitted light, without
93 knowing the spatial distribution of the light transmitance) can be sufficient.
94 From a scientific point of view, there is a need to identify the key elements of
95 plant architecture that are necessary to consider to correctly predicts different
96 processes including light transmission, at different scales. Indeed, "simplifications

97 which are unacceptable at a detailed level of representation can become
98 acceptable at a more integrated level (Tardieu, 2010). However the difficulty is to
99 define what the key elements are and the emerging properties linked to them
100 related to such or such a scale of description.
101
102 Mµslim is a model especially designed to bridge the gap between the statistical
103 and explicit approach. It can be seen as a multi-scale mixed model in the sense
104 that the light interception estimation method can be changed at each scale (Da
105 Silva *et al.* 2008). Furthermore, Mµslim was designed to to work with any type of
106 envelope encompassing the vegetation for which light attenuation is to be
107 computed, thus allowing precise description of complex canopy and crown
108 shapes. This feature allowed to overcome the restriction to analytically defined
109 envelope used in other models (Norman and Welles, 1983; Cescatti 1997).
110 Although it was initially dedicated to study light interception by isolated trees, its
111 versatile design and multi-scale approach made its adaptation to use at canopy
112 scale easy. Therefore we were able to use it to analyse how the deterioration of the
113 canopy description influences the accuracy of the light histogram simulated at the
114 plot level. Our objective was to specify the minimum field data needed by the
115 model to be able to accurately simulate the light distribution. Our experimental
116 design was as follow, 1) compare the simulated light distribution using the more
117 detailed description of the canopy with measured data on the field, 2) analyze the
118 statistical distance between histograms simulated for decreasing levels of

description and measured data.

Material and Method

1. Forest sites and plots

Three forest sites located in France with a total of 8 plots were used with increasing canopy structure complexity; 5 monospecific even-aged stands made up from *Pinus sylvestris* L. or *Pinus nigra* Arnold, 2 mixed *Quercus petraea* L. - *Pinus sylvestris* L. uneven-aged stands and 1 mixed *Abies alba* – *Pinus sylvestris* – *Fagus sylvatica* L. uneven-aged stands (Tab.1).

The Scots pine stands are located in the Chaîne des Puys, a mid-elevation volcanic mountain range at a place named Fontfreyde (Tab. 1). The elevation is 900 m a.s.l., mean annual rainfall is about 820 mm, and mean annual temperature is about 7°C. The soil is a volcanic brown soil at pH 6.0 with no mineral deficiency. The pines were 30 to 50-year-old at time of measurement, with a density ranging from 500 to 2300 stem ha^{-1} (Tab. 1). They are mainly regular even-aged stands. Some other species can be locally present such as *Betula pendula*.

The mixed oak – pine stands are located in the National forest of Orleans, in the sub-part named Lorris. They are typical stands of temperate plain forest with a mild climate (mean annual rainfall 720 mm; mean annual temperature 10.8°C) and acidic sandy poor soils temporarily flooded in winter or spring. They are irregular uneven-aged stands. Median DBH are about 18 cm, whereas some individuals, in particular of Scots pine, can reach 70 cm. Some other species are

141 locally present such as *Betula* sp., *Carpinus betulus*, *Sorbus torminalis*, *Malus*
142 *sylvestris* or *Pyrus communis.*
143 The third site is located in the South-East of France, in the mountainous area
144 named Mont Ventoux. One plot, VentouxC7, on the southern side of the
145 mountain, 1100 m a.s.l., is an old even-aged *Pinus nigra* plantation, almost
146 regular, with some pine and beech seedlings, on a flat area. The second plot,
147 Ventoux34, on the northern side of the mountain, 1400 m a.s.l., is a mixed
148 irregular stand with advanced regeneration of *Abies alba* and *Fagus sylvatica* with
149 some taller saplings almost reaching the open overstorey of old planted *Pinus*
150 *sylvestris*, and some other scattered species (*Sorbus aria, Acer opalus …).* The
151 climate is mountainous with Mediterranean influences (mean annual temperature
152 is 8.6°C and 6.7°C, and mean annual rainfall is 1080 mm and 1360 mm, for
153 VentouxC7 and Ventoux34, respectively). The soils are a calcosol (VentouxC7)
154 and a colluvial rendosol (Ventoux34), 20 cm and 50 cm deep in average,
155 respectively, with a high stone content (50% and 75% resp.), both with a silty clay
156 texture, on a fissured limestone. The median DBHs approximate 38 and 15 cm
157 (for the first and the second plot respectively) with some trees reaching 50 cm.
158

159 **2. Canopy structure measurements**

160 All trees in a square area, the experimental unit (Fig.1a), of size approximately
161 three times the height of dominant trees, were identified (species), located by their
162 x, y coordinates, and measured for their total height and Diameter at Breast Height

(DBH). Top and bottom crown heights were also measured. Lateral crown extents was assessed by visually projecting to the soil its characteristic points (i.e. the points that better describe the crown irregularities) in, at least, four directions, but sometimes with more than 8 directions when necessary. The azimuth and distance of those points from trunk were then measured (Fig.1b and c).

3. Light measurements

The light measurements were conducted in the central zone of the experimental unit. The surrounding zone where dendrometric measures were done acts as a buffer zone accounting for the attenuation of the encompassing forest (Fig.1a.). The light measurements were achieved using a square grid composed of 64 PAR sensors, namely *Solems PAR/CBE 80* sensors. Each sensor was separated from its neighbour in both direction by 2 to 3.5m depending on the considered plot (i.e. depending on the mean size of the trees). This distance was set by previous computation based on geostatistics (data not shown) and so that two contiguous measurements (points) can be considered as independent. Light measurements were done for each plot during 24h during summer to take the full sun course into account. One additional PAR sensor, *Sunshine sensor BF2*, was positioned outside of the experimental unit in full light to measure global (total) and diffuse incident radiation. This extra sensor uses an array of photodiodes with a computer-generated shading pattern to measure incident solar radiation and the D/G ratio, i.e. the diffuse to global radiation ratio. Transmittance for each point in

185 the understorey is then computed as the ratio of light measured in the understorey
186 divided by the incident value. The D/G ratio is taken into account for simulating
187 the transmittance with the model.
188
189 **4. Model description**
190 Estimation of light transmission is a process that requires first the stand
191 reconstruction. Then, the light attenuation within each crown must be defined so
192 that the light model can compute the transmittance under the entire canopy.
193 ◦ Canopy reconstruction
194 From the dendrometric measurements on the field, a mockup of the stand is
195 generated. This generation involves the construction of a crown (and trunk) for
196 each tree of the stand and its positioning. To reconstruct the 3D envelopes of the
197 trees from the field measurements, we used the PlantGL library (Pradal *et al.*
198 2008). This library contains several geometric models, including different types of
199 envelopes and algorithms to reconstruct the geometry of plants at different scales.
200 In this work, we used the *skinned surface* which is a generalization of surface of
201 revolution with varying profiles being interpolated. The envelope of a skinned
202 hull is a closed skinned surface which interpolates a set of profiles $\{P_k, k = 0,...,$
203 $K\}$ positioned at angle $\{\alpha_k , k = 0, . . . , K\}$ around the z axis, where K is the
204 number of profiles used to generate the skinned surface. This surface is thus built
205 from any number of profiles with associated direction. In such case, a profile is
206 supposed to pass through common top and bottom points and at an intermediate

point of maximum radius, i.e. the height of the crown maximum width. Two shape factors, C_T and C_B, were used to describe the shape of the profiles above and below the maximum width. Mathematically, two quarters of super-ellipse of degree C_T and C_B were used to define the top and bottom part of the profiles, see Da Silva *et al.* (2008) for details. Note that our envelopes can be viewed as extension of Cescatti (1997)'s asymmetric hull with profiles in any direction instead of the restricted cardinal directions. Flexibility of our model enabled us to measure the most adequate profiles in case of irregular crowns. The 3D envelope of a tree was thus obtained using a skinned surface generated from profiles defined from an angle, a maximum width and its associated height and two shapes factors. The trunk of the tree was represented as a cylinder of DBH diameter, the height of the cylinder being set to the crown bottom height. The 3D representation of an experimental unit is presented in Fig.2.

- Estimation of light transmission

The light transmission under such reconstructed stand was computed using the multi-scale light interception model (MµSLIM) presented in Da Silva *et al.* (2008). For each direction of incoming light, a set of beams was cast and the attenuation of each beam through the canopy was estimated. In the present study, the model was a simple two-scale model where the porous envelopes of crowns constituted the finest scale and the stand, the coarser scale. In replacement of the delicate estimation of leaf area density (LAD), a global opacity value, p_{gl}, was associated with each envelope of the reconstructed stand, the trunks were

229 considered opaque organs, thus their opacity was 1. Crowns global opacity were
230 estimated from field photographs shooting vertically different parts of the crown.
231 Each image was digitized, segmented to black and white and then the pixels were
232 counted using *PiafPhotem* software (Adam *et al.*, 2006). The ratio of black pixels
233 to the total number of pixels yielded the opacity of the crown while the ratio of
234 white pixels to the total number of pixels produced the crown porosity, hence
235 porosity = 1 - opacity. However, the opacity of each individual crown was not
236 directly estimated using this method because the segmentation procedure still
237 required human intervention. Instead a global opacity value per species was
238 estimated over a sample of pictures (Tab.1). MµSLIM allowed then to compute
239 the light transmission of the canopy by considering the light attenuation of each
240 beam. The light attenuation for one beam is computed according to the opacities
241 of the crowns encountered along its trajectory and according to the path length
242 within each of these crowns. The porosity expression that takes the beam
243 travelling distance into account is related to *G* (Chen and Black 1992; Ross 1981;
244 Stenberg 2006), the extinction coefficient that depends on light direction and leaf
245 inclination distribution, and *LAD*, the leaf area density. It can be expressed as:

$$p = \frac{1}{\beta} \sum_{b \in B} \left(1 - \exp\left(-G.LAD.l_b \right) \right) , \quad (1)$$

246 where *B* is the set of beams *b*, β is its cardinality, and l_b is the path length of the
247 beam into the crown. To take this distance into account, we thus need to
248 determine the quantity *G.LAD*.

249 The global opacity value can be regarded as the result of opacity estimation using
250 Beer-Lambert law in a infinite horizontally homogeneous layer:

$$p_{gl} = 1 - \exp(-G.LAI) \quad (2)$$

251 This relation yields an expression for *G.LAI*, where *LAI* is the leaf area index. In
252 the case of crowns with a finite volume, *V*, the usual definition of *LAI* can be
253 extended to be expressed as a function of the total leaf area, *TLA*, and the
254 projected envelope area, *PEA* (Sinoquet *et al.* 2007)

$$LAI = \frac{TLA}{PEA}, \quad (3)$$

255 and since *LAD* is the ratio of total leaf area to crown volume,

$$LAD = \frac{TLA}{V}. \quad (4)$$

256 We can express *G.LAD* as

$$G.LAD = \frac{G.LAI.PEA}{V} = \frac{-\log(1-p_{gl}).PEA}{V}. \quad (5)$$

257 Using this *G.LAD* value with equation (1) naturally leads to a smaller envelope
258 opacity value than p_{gl}. This is due to the fact that the negative exponential of a
259 mean value is less than the mean of negative exponential values. Therefore a
260 numerical approximation was carried out using the value from equation (5) as the
261 starting value to speed-up convergence. The process stopped when the opacity
262 computed using equation (1) was equal to the global opacity within a user-defined
263 error, ε. This *G.LAD* approximation was done once for each crown and for each

direction, and stored for further usage. The crown opacity for each beam, p_b, was then computed using the expression

$$p_b = 1 - \exp(-G.LAD .l_b) . \quad (6)$$

The light transmission of the canopy along one direction was estimated by computing, for each beam, its total opacity resulting from its travelling through the canopy, i.e. possibly going through multiple crowns, see Da Silva *et al.* (2008) for algorithmic and computational details. Experimental conditions were simulated by using two sets of incoming radiation directions. The first set, for diffuse light, discretized the sky hemisphere in 46 solid angle sectors of equal area, according to the Turtle sky proposed by Den Dulk (1989). The directions used were the central direction of each solid angle sector. The second set, for direct light, was used to simulate the trajectory of the sun, and the directions were dependant of the location (latitude, longitude), the day of the year, and on the time step used for the sun course discretization (approx. 25 directions in this work). Each of these directions was associated with a weighting coefficients derived from the Standard Over Cast (SOC) distribution of sky radiance (Moon and Spencer 1942). The porosity is directly the ratio of transmitted light to incident light, a value of 1 means that all light goes through while a value of 0 means that no light goes through. The grey-level image constituted by the beam porosity values is therefore a shadow map of the canopy transmittance. For each defined direction, MµSLIM was used to compute the opacity values of the beams and to produce such an image in a plane orthogonal to the light. To ensure both results precision

and fast computation, a lineic density of 150 was used for the beam sampling (Da Silva *et al.*, 2008), thus generating 150 x 150 pixels images. The images were then projected on the ground and rotated according to the light directions azimuth. Images from each set of incoming radiation directions were merged by using the weighting coefficients producing two intermediate images, one for the integrated transmittance of diffuse light and one for the direct light. Finally, these two images were merged using the diffuse to total ratio, D/G, measured from the extra sensor in the field. The grey-level values of pixels, from 0 (black) to 1 (white), represented the transmittance classes simulated by MµSLIM. The simulated light transmittance of the central zone could then be compared to the field measurements.

5. Virtual experiments

To assess the effect of the deterioration of canopy description on the simulated light histogram, we generated five different types of mockups for each stand with decreasing amount of information on canopy architecture.

1. The *asymmetric* mockup where *all available dendrometric* data are used to generate asymmetric crowns.
2. The *simple mean* mockup where crowns are represented by simple geometric shapes, cones for pines, spheres otherwise, and where the radius of each shape is the *mean of the measured radii*.
3. The *simple max* mockup where crowns are represented by simple

307 geometric shapes, cones for pines, spheres otherwise, and where the radius
308 of each shape is the *maximum of the measured radii*.
309 4. The *allometric radius* mockup where crowns are represented by simple
310 geometric shapes, cones for pines, spheres otherwise, and where the *radius*
311 of each shape is obtained from *allometric relation with DBH*.
312 5. The *allometric* mockup where crowns are represented by simple geometric
313 shapes, cones for pines, spheres otherwise, and where the *radius* of each
314 shape and the *height* of cones are obtained from *allometric relation with*
315 *DBH*.
316 For every type of mockup, the values for the height of crown base and for the
317 height of the cones (except for the *allometric* type) are the measured ones.
318 Allometric relations were defined as linear model between DBH and mean radius
319 and, for pines, between DBH and height. The relations obtained from field
320 measurements data are described in Tab.2, and Fig.2 shows 3D reconstructions
321 using two different types of crown shapes.
322 To complement the attenuation effect of the buffer zone for low elevation
323 radiations, it was necessary to add an artificial cylindrical wall surrounding the
324 zone of interest. The wall was centered on the zone of interest with a radius of the
325 zone of interest size. The height of the wall was set to the mean base crown height
326 of trees in the zone of interest. The coefficient of transmission of the wall (i.e.
327 wall opacity) was calibrated using in silico simulation experiments with the stands
328 of one site and then validated using the other stands from independent sites.

329 Adequacy of this method will be discussed further on.

330

331 **6. Model estimation**

332 The model outputs were qualitatively and quantitatively compared to experimental
333 data. The qualitative estimations were carried out by comparing the light
334 transmittance Cumulative Distribution Functions (CDF) to determine over- and/or
335 under-represented light transmittance class. The quantitative estimations were
336 achieved with the Kolmogorov–Smirnov test (K-S test) and the absolute
337 discrepancy index, AD (Gregorius 1974; Pommerening 2006). The K-S test is a
338 non-parametric test for the equality of continuous, one-dimensional probability
339 distributions that can be used to compare two samples. It quantifies the maximum
340 distance between the empirical CDF of two samples. The null distribution of this
341 statistic is calculated under the null hypothesis that the samples are drawn from
342 the same distribution. The p-value of the K-S test represents the α level at which
343 the null hypothesis can be rejected (i.e. a p-value > 0.1 means that the null
344 hypothesis cannot be rejected at 10% or lower level).
345 The absolute discrepancy index is defined as:

$$AD = \frac{1}{2}\sum_{i=1}^{n}\left|s_i - s_i^{'}\right| \quad AD \in [0,1] \tag{7}$$

346 where n is the number of classes, s_i is the relative frequency in class i of the first
347 distribution, and s'_i is the relative frequency in class i of the second distribution.
348 AD is defined as the relative proportion that needs to be exchanged between the

classes if the first distribution were to be transformed into the second distribution. Correspondingly, 1-AD is the proportion common to both distributions, a value of AD = 1 means that both distributions have no common class, whereas AD = 0 signifies that the distributions are absolutely identical (Pommerening 2006).

Both quantitative analysis were carried out with light measurements as reference values and the results are shown in Tab.3.

Results

The comparison between the CDF of the measured light transmittance and the ones obtained with the different mockups, as shown in Fig.3, were used to qualitatively assess the quality of the model prediction and the effect of deterioration of crown shape description. The CDF provides an alternate representation to light transmittance histograms that facilitates comparison between different distributions. The importance of a specific light transmittance class is given by the slope of the CDF at that point, i.e. a non represented class will yield a null slope and the more substantial the class, the steeper the slope (Fig. 3). The classes of high importance will be titled as main classes whereas the classes of low significance will be designated as minor classes.

Simulation with asymmetric mockups

The light model using the asymmetric mockups was able to simulate light transmission distribution similar to the measurement with a level of confidence of

371 the K-S test above 5% for all stands except Fonfreyde5 (3%) and Fonfreyde1
372 (<1%). In that case, the mean comparison yielded a statistically significant
373 difference for the same two stands. However, the AD values were below 0.3 for
374 all stands with a mean of 0.21 (Tab.3).
375 In the case of Fonfreyde1, the measured transmitted light were almost evenly
376 distributed in only two light transmittance classes, [0-5] and [5-10]. The simulated
377 distribution showed the same two main classes with an unbalance in favor of the
378 [0-5] class. Although the p-value of the K-S test allowed to reject the hypothesis
379 that the measured and simulated light distribution were similar, the AD value was
380 below the mean value of all stands. The simulated transmittance of Fonfreyde2
381 were almost identical to the measured ones despite the missing [0-5] class in the
382 simulation (i.e. simulated CDF slope is null through entire [0-5] class). The best
383 values for both the p-value and AD were obtained for this stand. In the case of
384 Fonfreyde3 the difference in the standard deviation (Tab.3) between the measured
385 and simulated light distributions was a good indicator of the fact that the lower
386 and higher classes, [15-25] and [50-60] respectively, were not simulated to the
387 profit of the median classes [30-40] as shown by the *Asymmetric* CDF being
388 below and then above the CDF of measurements. On the contrary, in the case of
389 Fonfreyde5, the *Asymmetric* CDF started below and ended above the
390 measurement one, indicating that the median classes ([10-20]) were under
391 simulated to the benefit of the [30-35] class that did not appear in the
392 measurements and the [5-10] one that have very low substance. The highest AD

393 values were obtained for these two stands.

394 The simulated distributions for Lorris38 correctly rendered both the main and
395 minor classes with, however, a less pronounced peak for the [5-10] class
396 expressed by the more abrupt slope of the measured CDF. There were no missing
397 or extra classes simulated and the AD was just above the mean value. Similarly to
398 Lorris38, the main and minor classes of Lorris255 were correctly simulated
399 without any missing or extra classes. Within each group, main and minor, some
400 classes were under-represented to the benefit of the over-represented ones.
401 However these discrepancies were subsidiary as the very high p-value and the
402 below-the-mean AD attest. In the case of VentouxC7, the simulated distribution
403 reproduced the bell-shape of the measured one but with slightly heavier tails due
404 to the two extra classes on the sides of the distribution, [35-40] and [65-70]. Note
405 that the isolated [10-15] measured class was not simulated, as shown by the
406 advent of a proportion difference between measurements and simulation.
407 Similarly to Lorris255, a high p-value and a low AD were observed despite of
408 these differences. Finally, the simulated distribution for Ventoux34, whereas
409 correctly simulating the two main classes, [0-5] and [5-10] accounting for almost
410 70% of the transmittance distribution, increased the unbalance between them in
411 favor of the lowest one. The minor classes were adequately simulated but without
412 respecting the discontinuity shown in the measurements as indicated by the above-
413 mean AD.

414

Simulation with the simple mean mockups

Replacing the asymmetric by the *simple mean* mockups significantly reduced the p-values of the KS test, except for Fonfreyde1 and Fonfreyde3, but yielded AD values below 0.3, except for Fonfreyde5 and VentouxC7, that were similar to the ones obtained with the *asymmetric* mockups as shown by the slight increase of the mean AD to 0.24. The principal effect of this change of crown shape on the distributions of light transmittance compared to the distributions obtained with the *asymmetric* crowns was to reduce the most represented classes to the benefit of the minor ones. This was comparable to the crushing effect obtained on a Gaussian function by increasing its variance parameter. The variance increase was indeed observed for all stands but Lorris255 and interestingly, the two sample t-test indicated statistically significant differences for Fonfreyde5, VentouxC7 and Lorris255. This effect actually benefited Fonfreyde1, Fonfreyde3 and Lorris38 simulation results. The p-value increased and AD decreased significantly for Fonfreyde1 and Fonfreyde3, whereas for Lorris38, both values decreased.

Simulation with the simple max mockups

The *simple max* approach yielded light transmittance distributions that were significantly shifted to the lower transmittance classes, i.e. left shifted CDF (Fig. 3). This effect was visible on the simulation results of all stands but was less pronounced for Fonfreyde3 and VentouxC7. The dramatic increase of the AD mean value to 0.6 well illustrated this behavior but mean comparison was

437 sufficient to assess the importance of the discrepancies.

438

439 *Simulation with allometric mockups*

440 The use of the *allometric radius* and *allometric* mockups yielded similar results as
441 illustrated by comparable means and variances and similar mean AD values, 0.345
442 and 0.333, respectively. The effect of this change of crown shape on the
443 distributions of light transmittance was similar to the *simple mean* effect with the
444 addition of a slight shift toward higher transmittance classes, indicated by right
445 shifted CDF (Fig. 3). The p-values were significantly reduced except for
446 Fonfreyde1, Fonfreyde5 and Ventoux34, but only for Fonfreyde1 this increase of
447 the p-value was associated with a decrease of AD (Tab.3).

448

449 *Comparison between all simulations*

450 The AD results (Fig.4) show that the *asymmetric* mockups yielded the
451 distributions closest to the measurement, the *simple mean* approach deteriorated
452 slightly the results whereas the *simple max* approach had dramatic effect. Using
453 *allometric* crowns yielded results in between but closer to the *simple mean* ones.
454 These results confirmed the classification trend yielded by the two-sample t-test
455 analysis that showed no statistically significant differences between the
456 measurements and the *asymmetric* and *simple mean* approaches on one side,
457 between the two *allometric* approaches on the other side and showed the
458 segregation of the *simple max* one.

Discussion

Statistical considering

Our study on the impact of the deterioration of the accuracy of crown representation on simulated light transmission highlighted some statistical issues. In spatially explicit transmittance models, a spatially point to point comparison approach between measured and modeled transmittance generally shows little agreement because small errors in crown location, often coming from errors during field measurements, yields large local differences in transmittance (Mariscal *et al.* 2004), particularly when the proportion of direct radiation is important (Groot *et al.* 2004). However only considering a mean and variation around this mean (e.g. SD) could lead to some errors (e.g. underestimation of area fully lighted) due to distribution non centered on mean with sometimes a long tail or several modes. To avoid this problem we compared the simulated distribution of light transmittance to the measured ones using two different non parametric descriptors, the K-S test and the AD index.

Although commonly used, and mathematically well-founded, the K-S test showed some limitations when applied to peculiar distributions as the one from Fonfreyde1. The problem stems directly from the test definition where the accordance between two distributions is based on the maximum distance between the CDFs. When the distribution shows very low dispersion, a small difference in

481 distribution can yield a big maximum distance between CDFs and therefore a
482 rejection of the null-hypothesis from K-S test. On the contrary, the AD index that
483 measures the changes required to transform one distribution into the other is
484 robust in regard of the distribution dispersion. Even though AD is very well suited
485 to quantify the difference between distributions or to classify results, the AD value
486 is not associated with any confidence index. Hence it is up to the user to define the
487 threshold under which distributions will be considered similar. Consequently,
488 combining the use of the K-S test and the AD index allowed us to accurately
489 compare and assess the differences between simulated and measured light
490 distributions.
491
492 *Model evaluation*
493 The goal of the present study was not to validate, *stricto sensus*, the model
494 MµSLIM. Such an evaluation would require an independent data set of light and
495 tree measurements. Our objective was to evaluate the quality of light predictions
496 with increasing deterioration of the crown description. However the comparison
497 of light measurements (with 64 sensors regularly distributed on a square grid in
498 the plot) and the simulation with full asymmetric crown description (i.e. crown
499 radius extension in 4 to 8 directions + crown height and length) showed the good
500 quality of simulated light distribution (K-S p-value > 0.10 or AD <0.3). Results
501 are in the range of models using similar scales of description (e.g. Brunner 1998;
502 Cescatti 1997; Gersonde *et al.* 2004; Groot 2004; Mariscal *et al.* 2004; Stadt and

503 Lieffers 2000).

504 As pointed out by Norman and Welles (1983), the computation of beam path
505 lengths is a crucial procedure. Due to the multi-scale design of MμSLIM, in
506 addition to the possibility of using any type of envelope, an analytical resolution
507 as proposed by Norman and Welles (1983) or Cescatti (1997) was not an option.
508 This task was instead performed by ray tracing algorithms that determine and
509 analyse the path of each cast ray among the canopy crown shapes (Wang and
510 Jarvis, 1990). With the ever increasing computational power of graphic cards
511 available to high level operations, this formerly time consuming procedure can
512 now be executed for many direction without impairing the model performances.

513

514 To avoid the problem of low elevation angles ; i.e. interception of light by very far
515 elements close to the horizon in the field, whereas not represented in the model,
516 we had to come up with an alternative to the classical solution of canopy
517 duplication or projection on torus. These approaches are based on the strong
518 assumption of canopy homogeneity ; using them with our strongly heterogeneous
519 stands would introduce a non controlled approximation that would, in turn, induce
520 bias in the results interpretation. Instead we chose to estimate the radiative
521 parameters of the surrounding environment using an inverse modeling approach
522 through the addition of an opaque wall. The wall opacity was calibrated using
523 Fonfreyde stands data with full asymmetric crown description. The value was then
524 used as a parameter to run the simulations for the stands from the two other

525 independent sites at the same level of crown description. Finally, the model
526 predictions were compared to the field light measurements. The results suggest
527 that the coefficient of transmission of the wall properly represented the radiative
528 properties of the environment, at least for low elevation angles. Moreover,
529 considering our objective, the opaque wall approach provided a simple solution
530 saving significant computational time otherwise required by the canopy
531 duplication. This approach seems thus promising and simple to set-up but would
532 benefit from more complete sensitivity analysis, in particular on wall size or
533 position.
534 One interest of our model is that crown porosity is simply estimated by a vertical
535 photograph of tree crown (extension of the method of Canham *et al.* 1999) and
536 seems to support accurate results in light distribution; however the extent to which
537 this parameter influenced the results needs to be more adequately studied. As
538 pointed out by Stadt and Lieffers (2000) determination of leaf and shading
539 elements (branch, trunk) is often critical in light transmission modeling.
540
541 *Effects of crown description deterioration*
542 Our results corroborate that differences in crown shape and size is a key
543 determinant of light transmittance as stated by Vieilledent *et al.* (2010). Moreover,
544 this study confirmed the importance of crown shape when simulating spatialized
545 light transmittance and endorse the sensitivity to variations in the crown geometry
546 parameters, especially the crown radius parameter, as already reported (Beaudet *et*

547 *al.* 2002; Brunner 1998; Cescatti 1997). However a crown mean radius with
548 crown height and spatialization seem to be a good alternate (Courbaud *et al.* 2003)
549 to detailed measures (i.e. measurement of crown extension in 4 to 8 directions)
550 even though simple shape like spheres and cones are known to be inadequate
551 (Mariscal *et al.* 2004). Other shapes should be tested, more in relation with tree
552 species architecture. Simplifying the crown representation in the tRAYci model to
553 average values for species and canopy strata resulted in little reduction in the
554 model performance (Gersonde *et al.* 2004). Describing tree crown extension with
555 4 to 8 radius is typically non feasible in practice in management or inventory
556 operations, whereas assessing mean crown diameter may be acceptable in some
557 cases. Therefore an approach that starts with simple shapes that can later be
558 deformed using an optimization process (Boudon and Le Moguedec 2007; Piboule
559 *et al.* 2005) should be considered in further studies. Indeed previous studies
560 showed the importance of crown asymmetric plasticity in response to local light
561 availability and space, among other factors (Vieilledent *et al.* 2010 and references
562 in it).
563
564 However using an *Allometric* approach would be more comfortable. The problem
565 is that the use of relationships between tree DBH and crown diameter or crown
566 height often decreased transmittance distribution prediction, whereas not for all
567 stands. With the allometric approach, the model generated smaller crown than
568 *simple mean*, thus same effect with shift to higher transmittance. We only tested

linear relationships and non-linear functions could have led to slightly better results (Beaudet *et al.* 2002) ; however many authors pointed out that the predictive functions for crown radius from e.g. DBH has proved elusive (Stadt *et al.* 2000) as they are often highly affected by uncontrolled factors such as climate hazards, stand density, or thinning operations (as probably reflected in the Fontfreyde's plots). There is often a high variability in tree allometry from an individual to another (Vieilledent *et al.* 2010). Actually the R^2 of the relationships linking crown diameter to trunk diameter in that study are not excellent but in the range of those commonly found in other studies (e.g. about 0.7 in Pinno *et al.* 2001 or Pukkala *et al.* 1993).

Effects of the stand complexity

High light variability is generally recorded in forests due to temporal variations of the sun path and heterogeneous spatial arrangement of light intercepting elements in irregular and/or mixed stands (Courbaud *et al.* 2003; Pukkala *et al.* 1993). In stands with a clumped structure (i.e. tree clumps alternating with large gaps), only an approach at tree scale with spatialization can correctly predict transmittance, whereas in dense stands, a Beer-Lambert law can be applied at the stand canopy scale (Balandier et al., 2010). It is however important to note that in dense stands, importance of small gaps within tree crowns due to different causes (diseases, broken branches, not taken into account in the simulation) can lead to noticeable differences as such of Fontfreyde 1 (Fig.3) (Beaudet *et al.* 2002). Low density

591 stands Fonfreyde3 and VentouxC7 are less affected by the *simple max approach*
592 probably because the crown “increase” is not enough to fill the 'big' gaps in the
593 canopy. Problems of crown overlaps, in fact very difficult to quantify in the field,
594 are also probably less critical than in dense stands.
595 As already pointed out by Courbaud *et al.* (2003) or Balandier *et al.* (2010) the
596 problem is that it is very difficult to generalize results recorded on a site for a
597 particular stand structure to other sites or stands with other species or structures.
598 This argues in favor of studying the effect of stand structure in interaction with the
599 scale of stand description; this could be done for instance by the use of point
600 process analysis.
601

602 ## Acknowledgements

603 The authors would like to thank for their help, in the field or for information on
604 the stands, Catherine Menuet, Gwenael Philippe, Philippe Dreyfus, and Yann
605 Dumas.
606

607 ## Funding

608 The study was partly supported by the French program “ECOGER”, sustainable
609 management of mixed forests.
610

611 ## References

612 Adam B, Benoît JC, Balandier P, Marquier A, Sinoquet H (2006) PiafPhotem -

613 software for thresholding hemispherical photographs. Version 1.0. UMR PIAF
614 INRA-UBP, Clermont-Ferrand - ALLIANCE VISION Montélimar, France.
615
616 Balandier P, Collet C, Miller JH, Reynolds PE, Zedacker SM (2006a) Designing
617 forest vegetation management strategies based on the mechanisms and dynamics
618 of crop tree competition by neighbouring vegetation. Forestry 79, 1: 3-27.
619
620 Balandier P, Marquier A, Dumas Y, Gaudio N, Philippe G, Da Silva D, Adam B,
621 Ginisty C, Sinoquet H (2009) Light sharing among different forest strata for
622 sustainable management of vegetation and regeneration. In: Orlovic S (ed)
623 Forestry in achieving millennium goals, Institute of lowland forestry and
624 environment, Novi-Sad, Serbia, pp 81-86.
625
626 Balandier P, Marquier A, Perret S, Collet C, Courbeau B (2010) Comment estimer
627 la lumière dans le sous-bois forestier à partir des caractéristiques dendrométriques
628 des peuplements. Rendez-Vous Techniques ONF 27-28: 52-58.
629
630 Balandier P, Sonohat G, Sinoquet H, Varlet-Grancher C, Dumas Y (2006b)
631 Characterisation, prediction and relationships between different wavebands of
632 solar radiation transmitted in the understorey of even-aged oak (*Quercus petraea*,
633 *Q. robur*) stands. Trees 20: 363-370.
634

635 Bartelink HH (1998) Radiation interception by forest trees: a simulation study on
636 effects of stand density and foliage clustering on absorption and transmission.
637 Ecol Model 105: 213-225.
638
639 Beaudet M, Messier C, Canham C (2002) Predictions of understorey light
640 conditions in northern hardwood forests following parameterization, sensitivity
641 analysis, and tests of the SORTIE light model. For Ecol Manage 165: 235-248.
642
643 Boudon F, Le Moguedec G (2007) Déformation asymétrique de houppiers pour la
644 génération de représentations paysagères réalistes. Revue Electronique
645 Francophone d'Informatique Graphique (REFIG) 1, 1.
646
647 Brunner A (1998) A light model for spatially explicit forest stand models. For
648 Ecol Manage 107: 19-46.
649
650 Canham C, Coates KD, Bartemucci P, Quaglia S (1999) Measurement and
651 modeling of spatially explicit variation in light transmission through interior
652 cedar-hemlock forests of British Columbia. Can J For Res 29: 1775-1783.
653
654 Cescatti A (1997) Modelling the radiative transfer in discontinuous canopies of
655 asymmetric crowns. I. Model structure and algorithms. Ecol Model 101: 263-274.
656

657 Cescatti A (1997) Modelling the radiative transfer in discontinuous canopies of
658 asymmetric crowns. II. Model testing and application in a Norway spruce stand.
659 Ecol Model 101: 275-284.
660
661 Chen JM, Black TA (1992) Defining leaf area index for non-flat leaves. Plant Cell
662 Env 15: 421-429.
663
664 Courbaud B, de Coligny F, Cordonnier T (2003) Simulating radiation distribution
665 in a heterogeneous Norway spruce forest on a slope. Agr For Meteor 116: 1-18.
666
667 Da Silva D (2008) Caractérisation de la nature multi-échelles des plantes par des
668 outils de l'analyse fractale, application à la modélisation de l'interception de la
669 lumière. Dissertation, University of Montpellier, France.
670
671 Da Silva D, Boudon F, Godin C, Sinoquet H (2008) Multiscale Framework for
672 Modeling and Analyzing Light Interception by Trees. Multiscale Modeling &
673 Simulation 7: 910-933.
674
675 Den Dulk JA (1989) The interpretation of Remote Sensing, a feasibility study.
676 Dissertation, University of Wageningen, The Netherlands.
677
678 Gaudio N, Balandier P, Dumas Y, Ginisty C (2011) Growth and morphology of

679 three forest understorey species (*Calluna vulgaris*, *Molinia caerulea* and
680 *Pteridium aquilinum*) according to light availability. For Ecol Manage 261: 489-
681 498.
682
683 Gersonde R, Battles JJ, O'Hara KL (2004) Characterizing the light environment in
684 Sierra Nevada mixed-conifer forests using a spatially explicit light model. Can J
685 For Res 34: 1332-1342.
686
687 Gregorius HR (1974) Genetischer Abstand zwischen Populationen. I. Zur
688 Konzeption der genetischen Abstandsmessung (Genetic distance among
689 populations. I. Towards a concept of genetic distance measurement). Silvae
690 Genetica 23: 22-27.
691
692 Groot A (2004) A model to estimate light interception by tree crowns, applied to
693 black spruce. Can J For Res 34: 788-799.
694
695 Hale SE, Edwards C, Mason WL, Price M, Peace A (2009) Relationships between
696 canopy transmittance and stand parameters in Sitka spruce and Scots pine stands
697 in Britain. Forestry 82, 5: 503-513.
698
699 Lieffers VJ, Messier C, Stadt KJ, Gendron F, Comeau PG (1999) Predicting and
700 managing light in the understory of boreal forests. Can J For Res 29: 796-811.

701

702 Mariscal MJ, Martens SN, Ustin SL, Chen J, Weiss SB, Roberts DA (2004) Light-
703 transmission profiles in an old-growth forest canopy: simulation of
704 photosynthetically active radiation by using spatially explicit radiative transfer
705 models. Ecosystems 7: 454-467.
706
707 Monsi M, Saeki T (1953) Uber den Lichtfaktor in den Pflanzengesellschaften und
708 seine Bedeutung fur die Stoffproduktion. Japanese Journal of Botany 14: 22-52
709
710 Moon P, Spencer DE (1942) Illumination from a non-uniform sky. Transactions
711 of the Illumination Engineering Society 37.
712
713 Myneni RB, Ross J, Asrar G (1989) A review on the theory of photon transport in
714 leaf canopies. Agr For Meteor 45:1-153
715
716 Norman J.M., Welles J.M. (1983) Radiative Transfer in an array of Canopies.
717 Agronomy Journal 75: 481-488.
718
719 Perrin H (1963) Sylviculture. Ecole Nationale des Eaux et des Forêts, Nancy,
720 France, Tome 1, p 174.
721
722 Pinno BD, Lieffers VJ, Stadt KJ (2001) Measuring and modelling the crown and

723 light transmission characteristics of juvenile aspen. Can J For Res 31: 1930-1939.
724
725 Pommerening A (2006) Evaluating structural indices by reversing forest structural
726 analysis. For Ecol Manage 224: 266-277.
727
728 Pradal C, Dufour-Kowalski S, Boudon F, Fournier C, Godin C (2008) OpenAlea:
729 a visual programming and component-based software platform for plant
730 modelling. Funct Plant Biol 35.
731
732 Pukkala T, Kuuluvainen T, Stenberg P (1993) Below-canopy distribution of
733 photosynthetically active radiation and its relation to seedling growth in a boreal
734 Pinus sylvestris stand. Scand J For Res 8: 313-325.
735
736 Ross J (1981) The radiation regime and the architecture of plant stands. The
737 Hague, The Netherlands.
738
739 Sillion FX, Puech C (1994) Radiosity and Global Illumination. The Morgan
740 Kaufmann Series in Computer Graphics, Morgan Kaufmann Inc. San Francisco,
741 California, USA
742
743 Sinoquet H, Stephan J, Sonohat G, Lauri PE, Monney P (2007) Simple equations
744 to estimate light interception by isolated trees from canopy structure features:

745 assessment with three-dimensional digitized apple trees. New Phytol 175: 94-106.
746
747 Song C, Band LE (2004) MVP: a model to simulate the spatial patterns of
748 photosynthetically active radiation under discrete forest canopies. Can J For Res
749 34: 1192-1203.
750
751 Sonohat G, Balandier P, Ruchaud F (2004) Predicting solar radiation
752 transmittance in the understory of even-aged coniferous stands in temperate
753 forests. Ann For Sci 61: 629-641.
754
755 Stadt KJ, Lieffers VJ (2000) MIXLIGHT: a flexible light transmission model for
756 mixed-species forest stands. Agr For Meteor 102: 235-252.
757
758 Stenberg P (2006) A note on the G-function for needle leaf canopies. Agr For
759 Meteor 136: 76-79.
760
761 Tardieu F (2010). Why work and discuss the basic principles of plant modeling 50
762 years after the first plant models? J. Exp. Bot., 61:2039-2041.
763
764 Vieilledent G, Courbaud B, Kunstler G, Dhôte JF, Clark JS (2010) Individual
765 variability in tree allometry determines light resource allocation in forest
766 ecosystems: a hierarchical Bayesian approach. Oecologia 163: 759-773.

767

768 Wang YP, and Jarvis PG (1990) Description and validationof an array model -

769 MAESTRO. Agr For. Meteor 51: 257-280.

770 # Tables

771

772

773

Table 1: Plot description. Each plot was approximately 50m x 50m

Site	Latitude Longitude	Elevation (m)	Density (stem ha^{-1})	Mean Height (m) (Min-Median-Max)	D.B.H. (cm) (Min-Median-Max)	Basal area (m^2 ha^{-1})	Tree species	Basal area (%)	Opacity
Fonfreyde1	47°42'N 02°58'E	920	2353	7.3 14.5 18.4	7 16 33	54	Pinus sylvestris Other species	99.4 0.6	0.835 0.75 – 0.86
Fonfeyde2	47°42'N 02°58'E	920	1103	7.2 14.5 18.3	7 17 42	33	Pinus sylvestris Other species	73.6 26.4	0.835 0.75 – 0.86
Fonfreyde3	47°42'N 02°58'E	920	563	6.3 14.2 18.2	9 21 37	22	Pinus sylvestris Other species	90.4 9.6	0.835 0.75 – 0.86
Fonfreyde5	45°41'N 02°59'E	910	710	11.3 18.3 23	9 28 43	42	Pinus sylvestris Other species	96.2 3.8	0.835 0.75 – 0.86
Lorris38	47°47'N 02°34'E	150	664	4 16.1 29.3	7 17 71	32	Pinus sylvestris Quercus petraea Other species	56.7 34.2 9.1	0.79 0.867 0.75 – 0.86
Lorris255	47°49'N 02°26'E	150	607	3.7 17 22.3	7 19 47	24	Pinus sylvestris Quercus petraea Other species	36.7 57.5 5.8	0.79 0.867 0.75 – 0.86

*Table 2: Allometric relation between DBH and crown mean radius and height. Linear models of the form a*DBH + b were used for both mean radius and height*

	Tree species	Site	Slope (a)	Intercept (b)	R^2
Mean Radius	Pinus	Fonfreyde	2.62	13.91	0.72
		Lorris	2.29	50.64	0.57
		Ventoux	1.86	69.28	0.83
	Quercus petraea	Lorris	2.73	129.69	0.60
	Fagus sylvatica	Ventoux	3.98	75.56	0.82
	Acer opalus	Ventoux	10.10	9.68	0.66
	Betula pendula	Fonfreyde	2.35	79.12	0.67
		Lorris	2.13	94.36	0.29
	Carpinus betulus	Lorris	7.18	74.78	0.36
	Populus tremula	Lorris	4.86	19.90	0.86
	Sorbus torminalis	Lorris	3.19	135.01	0.67
		Ventoux	2.88	85.38	0.71
Height	Pinus	Fontfreyde	0.08	10.09	0.47
		Lorris	0.10	10.27	0.64
		Ventoux	0.12	2.25	0.93

774

775

Table 3 Simulation results for the different mockups reconstruction. The p-value of the K-S test and the absolute discrepancy index (AD) were obtained with the measured light values as reference. Means with the same letter indicate that the difference between the means are not statistically significant at α=10% for an independent two-sample t-test.

Stand\Mockup		Measures	Asymmetric	Simple Mean	Simple Max	Allometric Radius	Allometric
Fonfreyde1	Mean	5.15[a]	4.19[b]	5.06[a]	0.44[c]	4.29[b]	4.14[b]
	Std	1.3	1.71	2.41	0.57	2	2.02
	p-value		1.3e-5	9.8e-3	<1e-5	7.1e-5	3.1e-5
	AD		0.203	0.063	0.516	0.141	0.172
Fonfreyde2	Mean	14.7[a]	14.69[a]	15.72[a]	7.19[c]	21.37[b]	20.32[b]
	Std	3.58	3.18	4.62	3.14	4.18	3.89
	p-value		0.987	0.05	<1e-5	<1e-5	<1e-5
	AD		0.078	0.219	0.75	0.594	0.531
Fonfreyde3	Mean	38.08[a,b]	37.05[a]	39.58[b]	25.81[c]	48.09[d]	43.18[e]
	Std	9.46	5.73	8.66	9.3	7.71	7.35
	p-value		0.08	0.52	<1e-5	1.3e-5	9.8e-3
	AD		0.281	0.234	0.453	0.406	0.329
Fonfreyde5	Mean	16.89[a]	19.29[b]	18.87[b,d]	9.52[c]	16.81[a,b,d]	18.32[a,d]
	Std	4.37	6.68	7.94	6.35	7.43	8.32
	p-value		0.03	0.017	<1e-5	9.8e-3	0.05
	AD		0.281	0.344	0.578	0.406	0.406
Lorris38	Mean	8.43[a]	8.41[a]	8.61[a]	0.645[c]	15.79[b]	16.09[b]
	Std	6.85	5.54	5.99	1.31	7.66	7.91
	p-value		0.126	0.029	<1e-5	1.9e-5	<1e-5
	AD		0.219	0.172	0.781	0.344	0.359
Lorris255	Mean	20.8[a]	21.33[a]	25.36[b]	5.49[c]	21.1[a]	21.1[a]
	Std	9.93	7.14	7.01	4.99	11.54	11.42
	p-value		0.758	0.029	<1e-5	0.16	0.203
	AD		0.172	0.25	0.844	0.281	0.266
VentouxC7	Mean	53.34[a]	54.3[a,b]	57.38[d]	47.72[c]	55.66[a,b]	54.87[b,d]
	Std	7.06	5.91	7.5	9.9	7.74	7.68
	p-value		0.52	2e-4	7e-5	0.005	0.017
	AD		0.172	0.359	0.375	0.266	0.281
Ventoux34	Mean	12.25[a,b]	8.87[a]	10.54[a]	3.44[c]	16.85[b]	17.05[b]
	Std	15.29	11.35	13.52	7.9	19.59	19.74
	p-value		0.05	9.8e-3	<1e-5	0.274	0.188
	AD		0.25	0.266	0.391	0.281	0.281

Captions of Figures

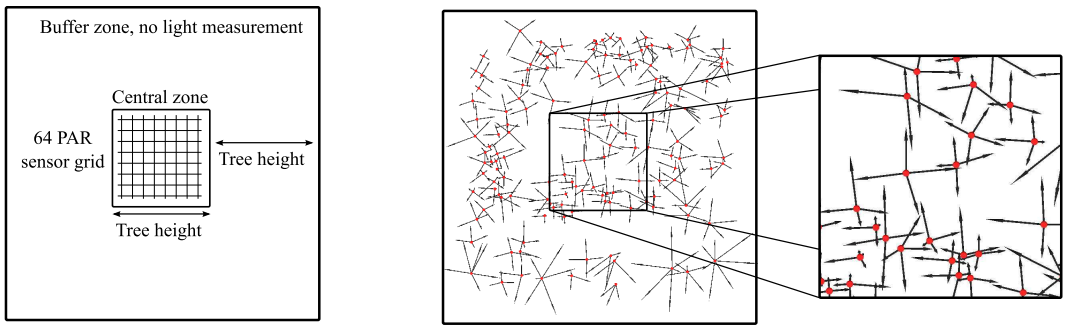

Figure 1: a. Experimental Unit. b. Field data: each dot locates a tree (its trunk), and each arrow defines a specific azimuth and distance from the trunk, characterizing the crown extend. c. Zoom in on the interest zone where light measurements where conducted.

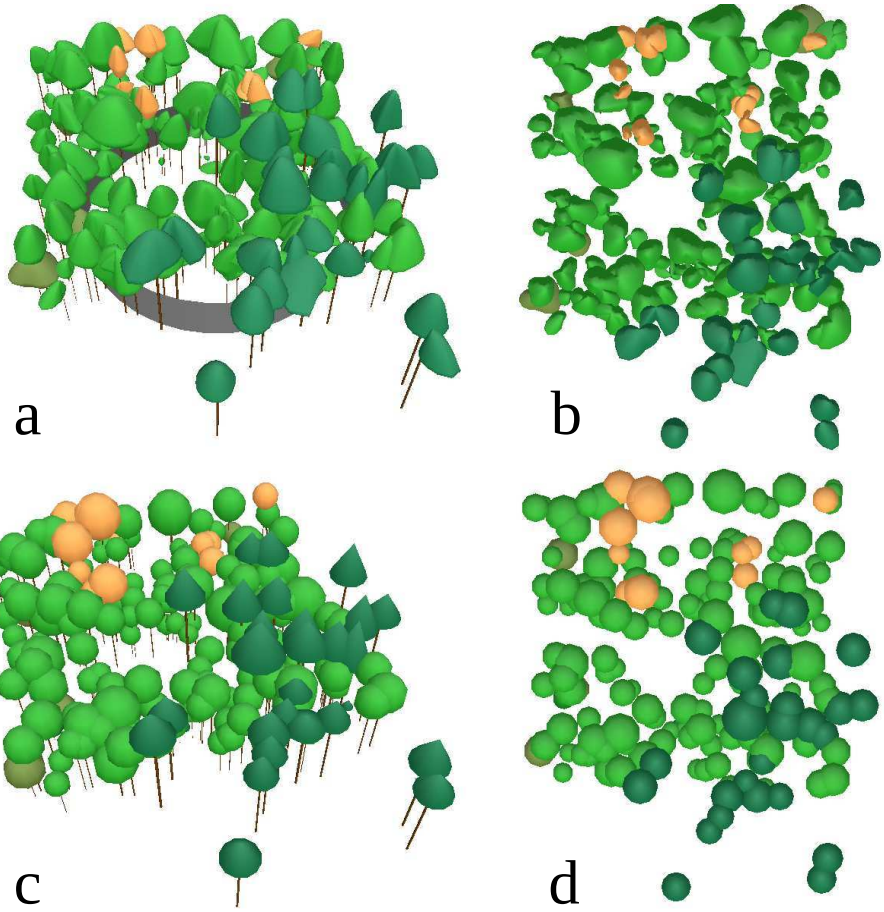

781

Figure 2: 3D reconstruction of the Lorris255 experimental unit using the asymmetric crowns, side view(a) and top view(b), and using the crowns from the allometric radius approach, side view(c) and top view(d) .Colors are used to visually differentiate between tree species: dark green for pine (Pinus sylvestris L.), green for oak (Quercus petraea L.), orange for birch (Betula L.), and brown for hornbeam (Carpinus betulus L.)

782

783

784

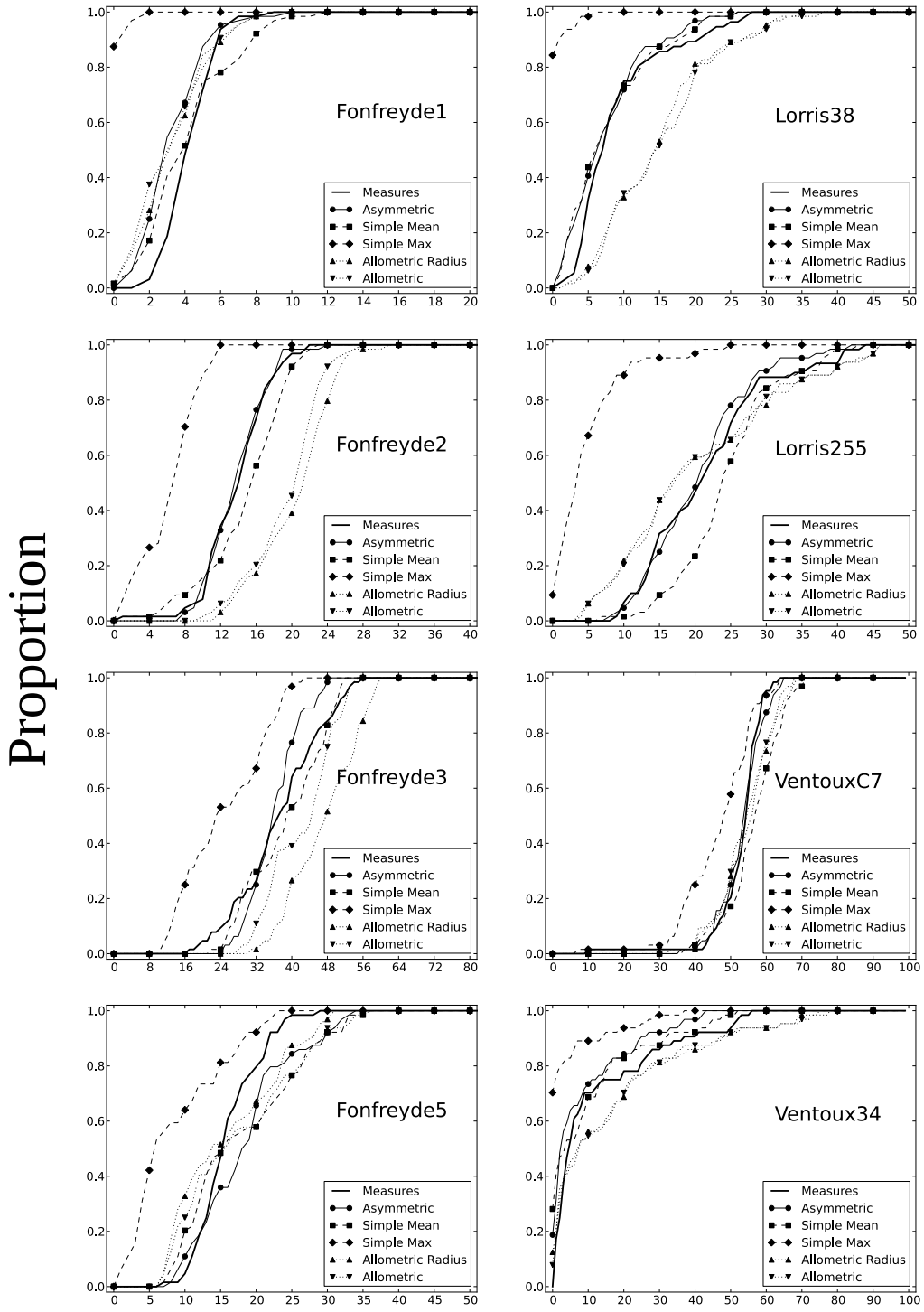
Fonfreyde1
Lorris38
Fonfreyde2
Lorris255
Fonfreyde3
VentouxC7
Fonfreyde5
Ventoux34
Measures
Asymmetric
Simple Mean
Simple Max
Allometric Radius
Allometric
Proportion
Transmittance (%)

785

Figure 3: Cumulative Distribution Function (CDF) of light transmittance for each stand and for every mockup type. Note that for legibility purpose the x-axis scale was adapted for each stand.

786

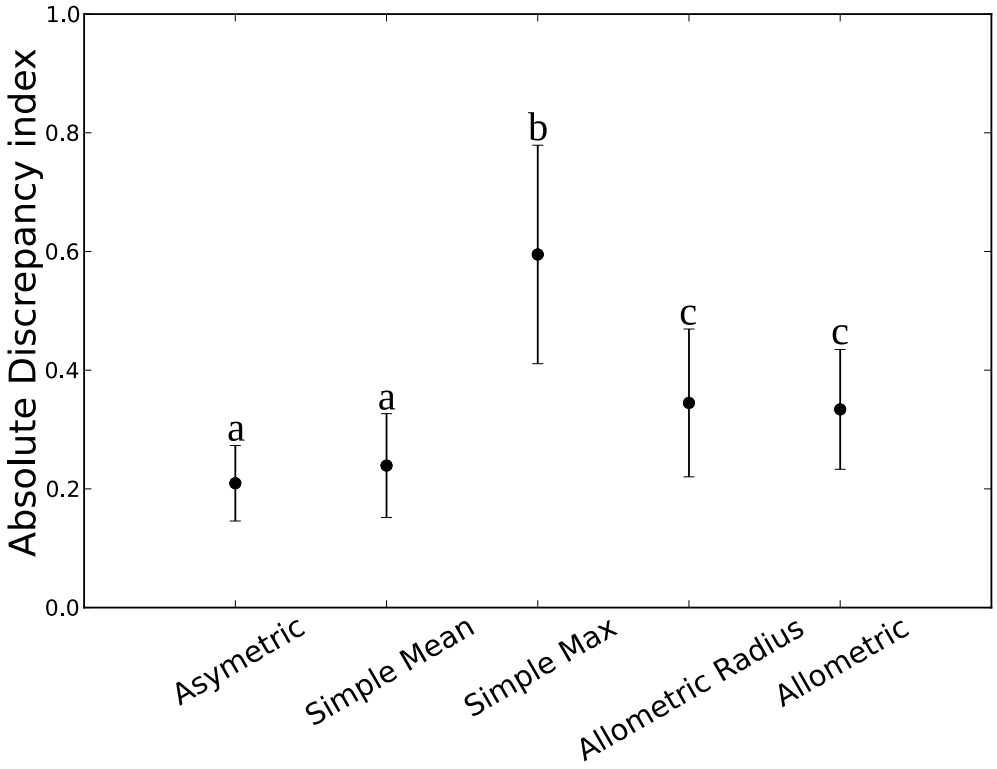

787

Figure 4: The points represent the mean of AD calculated for each type of mockup over all stands, the bars being the standard deviation. Same letter above the bars indicate that the difference between the means are not statistically significant at α=10% for an independent two-sample t-test.